Fracture of Skin/Stiffener Intersections in Composite Wind Turbine Structures

Douglas S. Cairns, Darrin J. Haugen
Department of Mechanical Engineering
and
John F. Mandell, Daniel D. Samborsky,
Department of Chemical Engineering
Montana State University-Bozeman
Bozeman, Montana 59717

Abstract

The strength of skin/stiffener intersections in composite wind turbine blades is a potential limiting factor in blade performance. To investigate the fracture of this region, an approach combining mechanical pull-off tests with finite element analysis (FEA) was used. The primary goals were to quantify and compare the damage initiation and propagation characteristics of various pull-off samples.

Pull-off tests were performed to compare the parameters of manufacturing method and bond-line thickness. Two types of "T" samples were investigated. The first resin transfer molded the skin and stiffener as a single unit. The second bonded the skin to the stiffener with an adhesive. The initial damage load was dependent on the manufacturing process, with the bonded samples tolerating higher loads than the one-piece specimens. Initial damage and ultimate loads increase with increasing adhesive thickness. However, it appears that this is due primarily to the increased bending stiffness caused by the thicker adhesive layers.

The FEA procedure involved modeling the pull-off samples with the ANSYS finite element code to calculate the strain energy release rates. The flange/skin interface crack changed from mixed mode I(opening) and II(shearing) growth to a dominantly mode I growth as the delamination grew from the specimen centerline toward the flange tip.

Introduction

Most wind turbine blades utilize a span-wise stiffening spar that is either co-cured or secondarily bonded to the inner skin surfaces. A potential problem with blades is debonding failure at this skin/stiffener intersection. Damage often initiates at this detail region, forming a delamination, which may lead to ultimate failure of the blade. In order to investigate the mechanisms and modes of failure for these structures an approach was used that combined experimental testing with finite element analysis. These analyses simulated the MSU- AOC 15/50 wind turbine blade in these detail regions (Fig.1). Two manufacturing methods under consideration for this fiberglass blade are using resin transfer molding (RTM) to make skins and a spar separately, followed by adhesive bonding, or to mold these intersections as one unit. As a result, parameters of interest are comparing bonded skin/stiffener intersections to an identical lay up molded as a single unit. This leads to subsequent comparison of the bonded sample strength versus adhesive thickness.

Experimental Procedure

Two different sample types were manufactured by RTM and tested. The first was a one-piece "T" sample with the spar and skin molded together. The second had the spar molded and cured separately from the skin. The spar was then bonded to the skin with an adhesive. The goals of the experimental procedure were to compare the relative performance of the one-piece RTM samples and the two-piece bonded stiffeners, and to investigate the failure modes in these tests. In addition, strength of the bonded stiffeners versus adhesive thickness was investigated.

The samples were made by RTM with a polyester matrix (CoRezyn 63-AX-051 with 2% MEKP catalyst), with E-glass fabric. Knytex D155 was used for the 0^0 layers (in-line with the z-axis Fig. 1), while the +/- 45 layers are a Knytex DB120. The dimensions of a typical test sample are shown in Figure 2. The lay-up of the skin and spar were identical in all of the samples tested, with a $[+45/-45/0/0/+45/-45]_S$ lay-up. Within the stiffening spar, half of the web was transitioned out to form either side of the flange portion (Fig.3a). The one-piece samples were

made by molding the skin and stiffener as a single unit. The two-piece samples were manufactured in the same mold with Teflon release film between the stiffener and skin. The two cured halves were then bonded together with Hysol EA 9309 adhesive. The average bond-line thickness for the first series of tests was 0.15 mm.

A noticeable change in thickness across the width of the skin under the flanges was seen after the samples had cured. This was due to the mold compressing the fabric layers in the skin underneath the flanges. A matrix burn-off test was performed to calculate the fiber volume fraction at a known thickness for the skin material away from the flange area. The fiber volume fraction could then be calculated across the width since the lay-up is constant across the width. The fiber volume varies from 30% to nearly 36% across the width. This should be noted, since the strength varies with the fiber volume percentage, especially in fatigue.[1] It was also noted that the fabrics had a difficult time negotiating the small bend radius (1.8 mm) where they transition from the web to the flange. This caused small resin pockets to form on the surface of the samples in the bend area (Fig. 3a).

The samples were tested in displacement control mode with the load applied to the web by clamping the upper 3 cm (Fig. 2). The skin was in contact with two circular bars at a support spacing of 12.7 cm (Fig. 2). Data was collected for load vs. deflection for subsequent analysis. In addition, the loads corresponding to various crack initiation and growth stages were manually recorded and checked against the load/deflection curves.

Experimental Results

The first series of tests involved comparison of the one-piece specimens to the samples bonded with adhesive. The same failure modes and sequences were seen in all of the samples. The first damage to appear was between the +/-45 plies at the bend surface, where the web transitions into the flange. This damage is labeled crack 1 in both the photograph of Figure 3b and the load vs. displacement curve (Fig. 4). The two load drops for crack 1 correspond to identical damage on the right and left sides of the sample. The next damage to appear is labeled as crack 2, and was a crack at the interface of the matrix rich "noodle" region and the inner -45 layer at the bend. Several more cracks formed in the noodle region, including cracks at the centerline of the web and the small resin pockets at the bend surface. This array of cracks eventually joined and moved downward to the flange/skin interface. The delaminations then began at this interface as well as the web centerline. The delamination lengths at the flange and web were nearly the same length in the x and y directions (Fig. 3a), respectively, throughout the test.

In the one-piece samples, the delamination formed either within the matrix layer at the skin/flange interface, or just below, within the skin's +45 top ply. This was also observed in the bonded samples. In addition, the delamination did not grow within the tougher adhesive layer. It formed below it at the interface, or within the topmost skin ply as seen in the one-piece samples. This is consistent with other findings in similar pull-off tests[2] and the fact that interlaminar strength tends to be dominated by matrix toughness.[3] Thus, the crack can more easily propagate within the brittle polyester matrix than in the tougher Hysol layer. The delamination continued to progress outward toward the flange tip in a stable manner until final pull-off when the crack was very near the flange tip.

A large amount of fiber bridging was observed in nearly all of the tests, especially for the one-piece samples. This has been shown to increase the toughness of composites.[4] Another observation is that the delamination always grew from the centerline (noodle region) outward toward the flange tip. In tests by other researchers, the delamination often starts at the flange tip and grows inward toward the centerline.[2] This may be due to the fact that the flange material in the current samples is quite thin and compliant. It has been shown that skin flexural stiffness has a large influence on pull-off strength, with stiffer samples tolerating higher loads.[2] It is likely that stiffer flange material will also increase the pull-off loads and change the damage initiation location from the bend region to the flange tip. This was, in fact, observed in later tests.

In composite design, and pull-off tests, two loads are of main interest: initial damage load, and maximum load. A summary of these values for the first series of tests are presented in Table 1. The main result worth noting is the difference in load at initial damage. The bonded samples tolerated an average load of 94 N/cm of sample width, while the one-piece samples were only about 71 N/cm, which was a 32% increase. The maximum load, however, showed little difference for the first tests, 124 N/cm versus 129 N/cm for the bonded and one-piece samples respectively.

The increase in initial damage load for the bonded samples is likely due to two factors. First is the slight increase in bending stiffness by the addition of the bond-line. Calculations from laminate analysis showed that the bending stiffness (D_{11}) for the skin and flange together increased from 211 N-m for the one-piece samples to 225 N-m for the 0.15 mm bond-line samples. The second factor is load redistribution caused by straining of the low modulus adhesive layer. This would lower the stress in the bend region at a given load compared to the one-piece samples.

The next step was to investigate the variation in strength

with bond thickness, which is shown in Figure 5. The graph indicates that initial damage load and ultimate load both increase with increasing bond-line thickness for the range of samples tested. However, as the thickness increases, the two load values converge, until they are the same value for the 6 mm bond samples. This implies that the thicker bond samples do not exhibit stable crack growth, and would give little or no warning between initial cracking and ultimate pull-off. The mode of failure also changed for the 6 mm bond samples. The initial damage occurred at the flange tip and moved inward toward to noodle region. This is likely due to the increased stiffness of the samples brought on by the very thick bond-line. D_{11} for the 6 mm bond tests was calculated as 1463 N-m.

To investigate the effects of bending stiffness further, two samples were made by bonding a thick $(45/-45)_{12}$ block to the standard flange to create a D_{11} (skin and flange) of 9903 N-m. The bond-line thickness for these flanges was approximately 0.2 mm. The average initial damage load increased to 147 N/cm and the maximum load to 184 N/cm for these samples. While this is well above the strength for the standard flange and 0.15 mm bond-line, it is less than the values for the 6.0 mm bond-line samples with the standard flange (D_{11} = 1463 N-m). This shows that the flange bending stiffness is not the only factor affecting pull-off strength. It also shows that increasing the flange stiffness, without changing the skin stiffness, does not increase pull-off strength indefinitely.

Analytical Procedure

The analytical procedure involved modeling the skin/stiffener with the ANSYS finite element code and calculating the strain energy release rates to grow the typical delamination observed experimentally.

To reduce solution time, only one half of the sample was modeled. This was possible since the sample deflection was symmetric about the vertical centerline. Eight-node quadrilateral elements (2-D) were used with an assumed plane strain condition. In the ply immediately above and below the delamination, two or three elements were used through each ply thickness. The rest of the model used one element per ply thickness.

To calculate the strain energy release rate (SERR) in modes I and II, the virtual crack closure technique[5] (VCCT) was used (Fig. 6). In this method, two solutions are needed. The first computer run loads the sample and opens the crack. In the second, unit loads are applied at nodes one element length behind the crack tip. The ratio of load to displacement is used to determine how much force it would take to bring the nodes back together, thus closing the crack. The advantage of this technique lies in

its ability to give good results with a fairly coarse mesh.

Analytical Results

A plot of the deflected shape for a sample containing a delamination is shown in Figure 7. The results of the SERR calculations are presented in Figures 8 and 9 for mode I and II contributions, as well as total SERR (G). Two distinct delaminations were investigated. The first crack was at the interface of the flange and skin. The second was located at the mid-plane of the web, growing vertically between the two inner -45^0 plies. The results are for delamination lengths greater than 1.2 cm, as measured from a point at the specimen centerline on the flange skin interface (Fig. 3a). The SERR results are calculated for the one-piece samples without the adhesive layer. Figure 8 shows that the total SERR is dominantly mode I as the delamination approaches the flange tip for the flange/skin crack. The maximum value for G_{Ic} is approximately 700 (J/m^2) per unit width. It also appears that the mode II contribution is greatest at small crack lengths near the noodle region. The vertical web crack is purely mode I due to the symmetry of the test. It has a relatively constant value of about 600 (J/m^2) per unit width (Fig. 9).

Due to the complex nature of the damage zone in the noodle region, it is difficult to calculate a SERR for the interface delamination at shorter lengths. This is because the interface delamination is not well defined until a certain distance away from the centerline.

Currently, double cantilever beam (DCB) and end-notched flexure tests (ENF) are underway to calculate experimental results for G_{Ic} and G_{IIc} for delamination growth at various interfaces in the E-glass/polyester material. This data will be compared with the FEA results to validate the models, and predict the growth of delaminations in the structures. Modeling of the complex damage zone in the noodle region is currently underway to establish a workable failure criteria for damage initiation and propagation in this area.

Summary and Conclusions

The effect of the manufacturing process and bond-line thickness on initial damage and maximum loads was presented. The first series of tests showed that the bonded skin/stiffeners (0.15 mm bond) tolerated a 32% greater load at initial damage versus the one-piece samples. The second series of tests evaluated the effect of increasing bond-line thickness on pull-off strength. In this case, both initial damage load and maximum load increased with increasing bond thickness. However, the two values converged as thickness increased. This indicates that there would be little stable crack growth for

the thicker bond-lines, and less warning between initial damage and ultimate failure. In addition, for the thickest bond-lines tested (> 6 mm), the failure initiated at the flange tip, rather than in the bend region. This is probably due to the increased bending stiffness of the samples with increasing bond-line thickness.

Based on the experimental observations, it appears that both bending stiffness and the addition of a low modulus adhesive layer will increase the damage loads in the pull-off samples. However, there is an upper limit to the influence of these parameters on strength with constant skin lay-up. These factors will be investigated further with finite element models and additional testing.

Once fracture occurred, a multi-crack damage zone developed in the web/flange transition region. Simultaneous delaminations at the flange/skin interface and web centerline then formed. They progressed from the noodle region toward the flange tip and upward in the web, respectively. The flange delamination grew at the adhesive/skin interface or within the topmost skin ply, not within the adhesive layer itself.

The noodle/bend region of the stiffeners appears to be a critical design detail. This area usually displayed the first damage in the samples. The bend is an obvious stress concentration in this type of structure. Furthermore, the fiberglass fabric used in manufacturing had a hard time conforming exactly to the bend radius. This caused resin pockets on the sample surface, as well as possible local fiber bunching and increased fiber volume percentage at the bend.[1,6,7] Bend radii of mold surfaces should be increased to lower the stress concentration and allow the fabric to conform to the bend surface more easily. Fiberglass tows should also be placed in the noodle area to raise the strength of this pure matrix region.

Based upon the previous results, it appears that adhesive bonds increase the fracture loads of skin/stiffener intersections in composite wind turbine blades. Careful attention should be given to surface preparation of the samples to achieve the full potential of the adhesive. If this is not done, the adhesive will likely peel of at the interface, with little surface interaction.

Future Work

Future work will continue to combine experimental testing with finite element analysis to investigate parameters of interest to the wind turbine industry. Samples will be produced in a mold with a variable radius insert. This will allow the stress concentration to be lowered and let the fabric conform to the bend more easily. Additional tests for the variation in strength with bond-line thickness and bending stiffness will be performed. Different adhesives will also be compared to the Hysol EA 9309 used in these samples for pull-off performance.

Additional loading cases will be tested including compressive testing and fatigue loading.

The damage initiation at the bend/noodle region will be modeled with ANSYS, and appropriate failure criteria will be developed and validated experimentally.

Finally, a database with skin/stiffener intersection design recommendations will be published for the wind turbine industry.

References

1. Mandell, J.F., Samborsky, D.F., Scott, M.E., and Cairns, D.S., "Effects of Structural Details on Delamination and Fatigue Life of Fiberglass Laminates", Wind Energy 1998, ASME/AIAA, January, 1998 (to be published).

2. Minguet, P.J., Fedro, M., et. al., "Development of a Structural Test Simulating Pressure Pillowing Effects in a Bonded Skin/Stringer/Frame Configuration", Proceedings, Forth NASA/DoD advanced Composites Technology Conference, Salt Lake City, UT, June 1993

3. Bradley, W.L., "Relationship of Matrix Toughness to Interlaminar Fracture Toughness", Application of Fracture Mechanics to Composite Materials, K. Friedrich Ed., Elsevier (1989)

4. Davies, P., and Benzeggagh, M.L., "Interlaminar Mode-I Fracture Testing", Application of Fracture Mechanics to Composite Materials, K. Friedrich Ed., Elsevier (1989).

5. Rybicki, E.F. and Kanninen, M.F., "A Finite Element Calculation of Stress-Intensity Factors by a Modified Crack Closure Integral." Engineering Fracture Mechanics, Vol. 9, pp.931-938. (1977).

6. Holmberg, J.A., and Berglund, L.A., "Manufacturing and Performance of RTM U-Beams", Composites Part A, Vol. 28 No. 6, pp. 513-521, Elsevier (1997).

7. Kedward, K.T., Wilson, R.S., and McLean, S.K., "Flexure of Simply Curved Composite Shapes", Composites, Vol. 20, No. 6, Butterworth & Co. (1989).
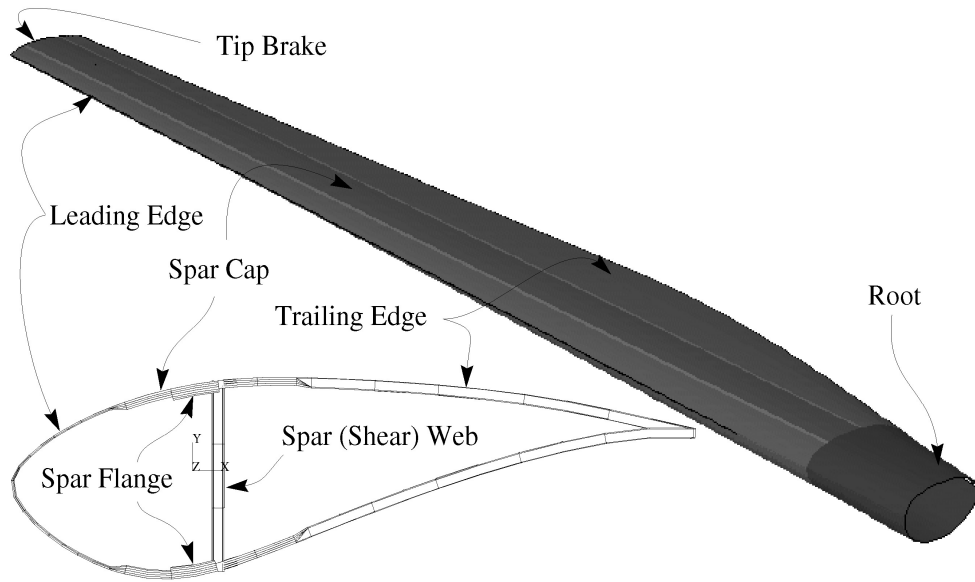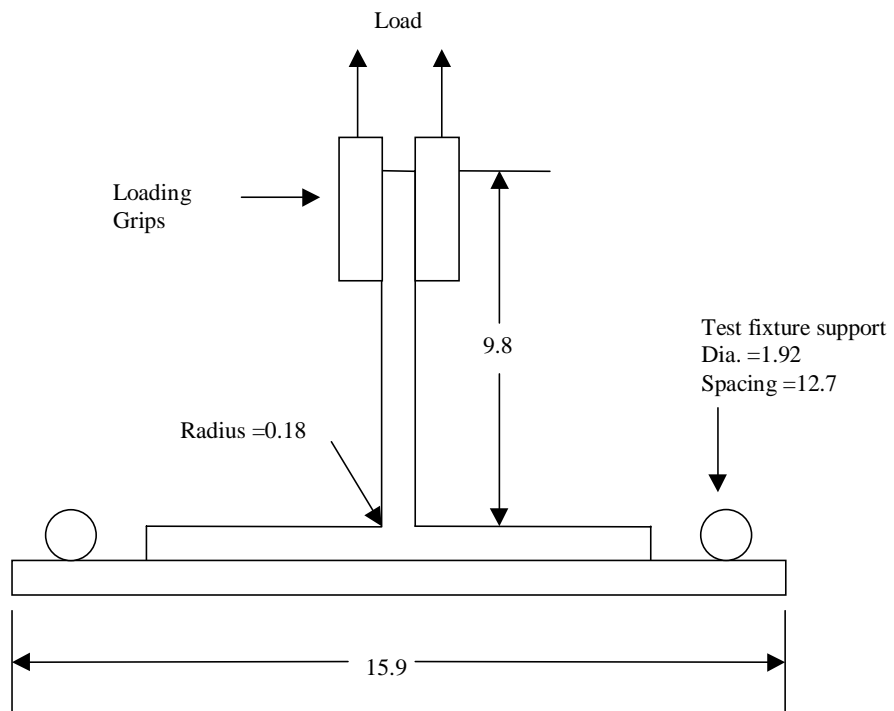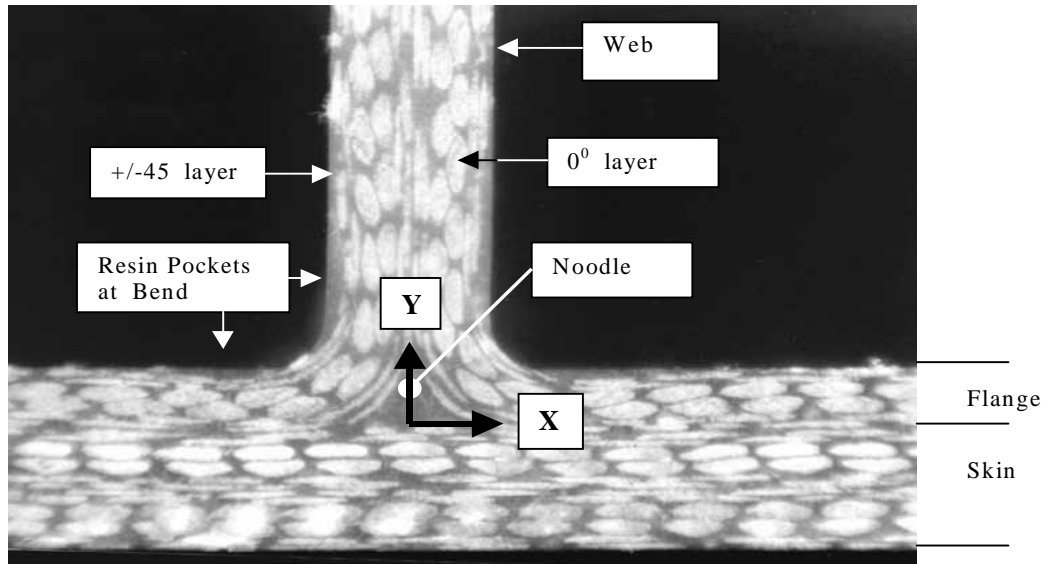
Tip Brake

Leading Edge

Spar Cap

Trailing Edge

Root

Spar (Shear) Web

Y
Z   X

Spar Flange

Figure 1.
overview and
section

Load

Blade
cross-

Loading
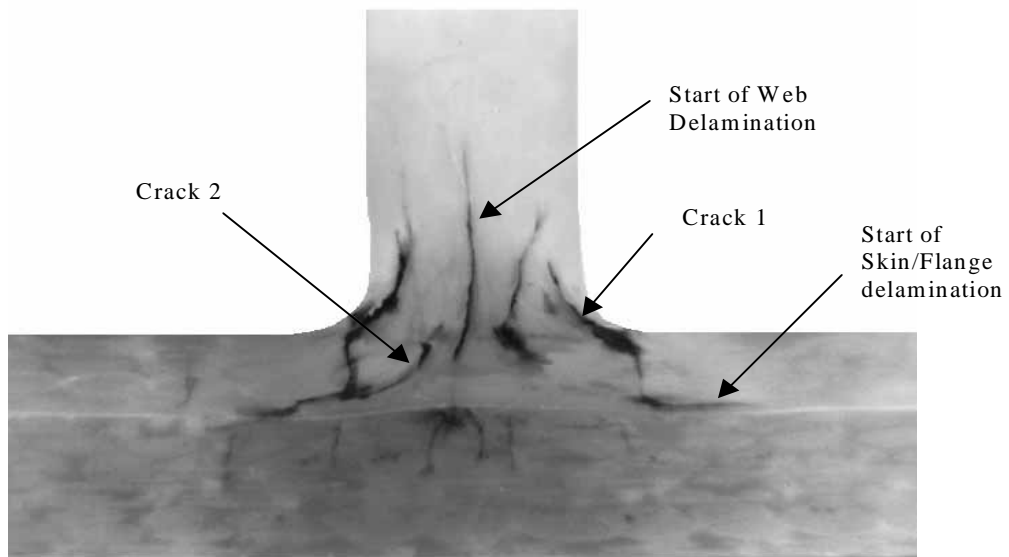Grips

9.8

Test fixture support
Dia. =1.92
Spacing =12.7

Radius =0.18

15.9

Skin thickness = 0.45
Web thickness = 0.47
Depth (into page)= 5.1
All dimensions in cm.

Figure 2. Test specimen with dimensions

Web

+/-45 layer

0^0 layer

Resin Pockets at Bend

Noodle

Y

X

Flange

Skin

a.

Start of Web Delamination

Crack 2

Crack 1

Start of Skin/Flange delamination

b.

Figure 3. Photo of specimen with (a) key features labeled, and (b) initial damage zone.

Typical Load vs. Displacement Curve for Pull-off Samples

Crack 2
Damage at noodle

Crack 3
Stable delamination growth

Crack 1
Damage at bend

0.15 mm bond thickness

Load (N/cm)
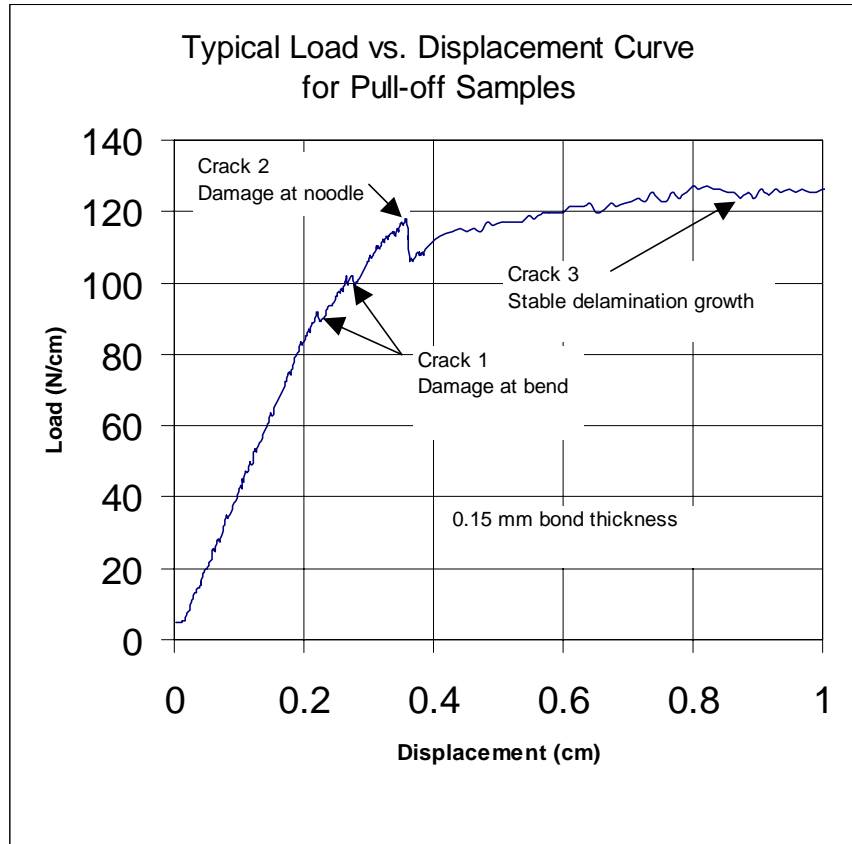
Displacement (cm)

Figure 4. Typical Load vs. Displacement curve with damage points labeled.

Table 1. Average Strength of Pull-off Samples

	One-Piece Stiffener	Two-Piece Bonded Stiffener
Initial Damage Load (N/cm width)	71.0	93.7
Maximum Load (N/cm width)	129.0	124.1
Number of Samples tested	4	5
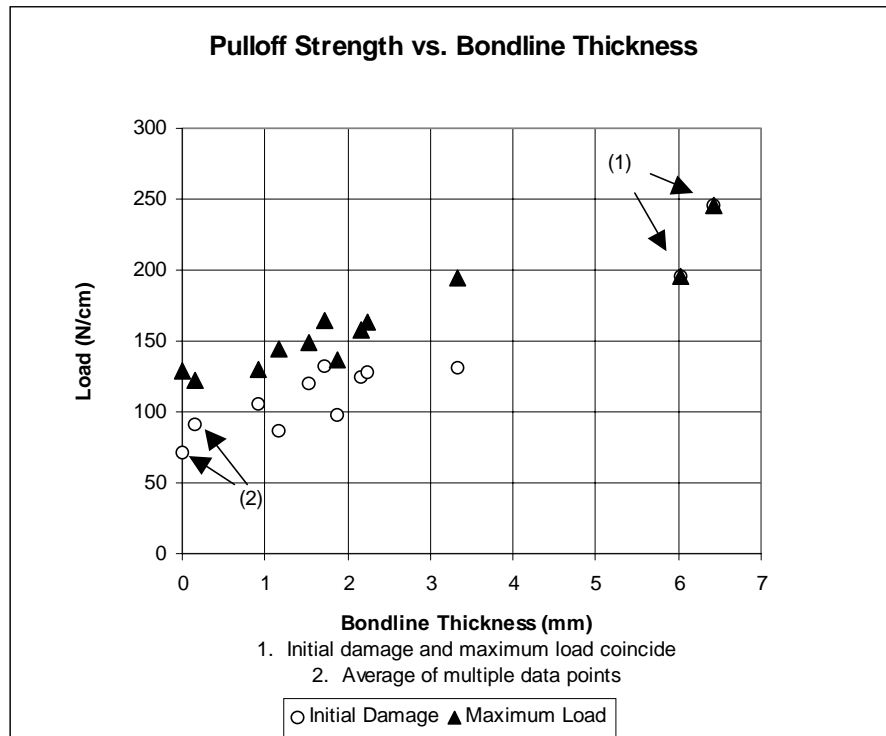
Figure 5. Strength vs. bond-line thickness.
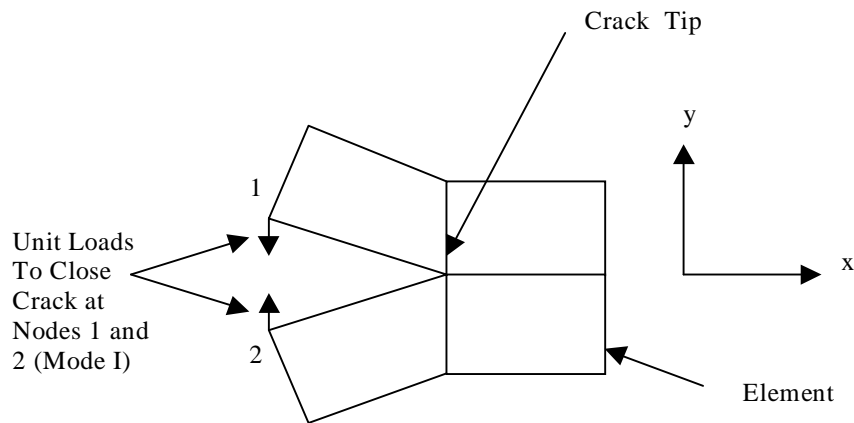
Figure 6. Two-step virtual crack closure technique (VCCT) to calculate strain energy release rate.
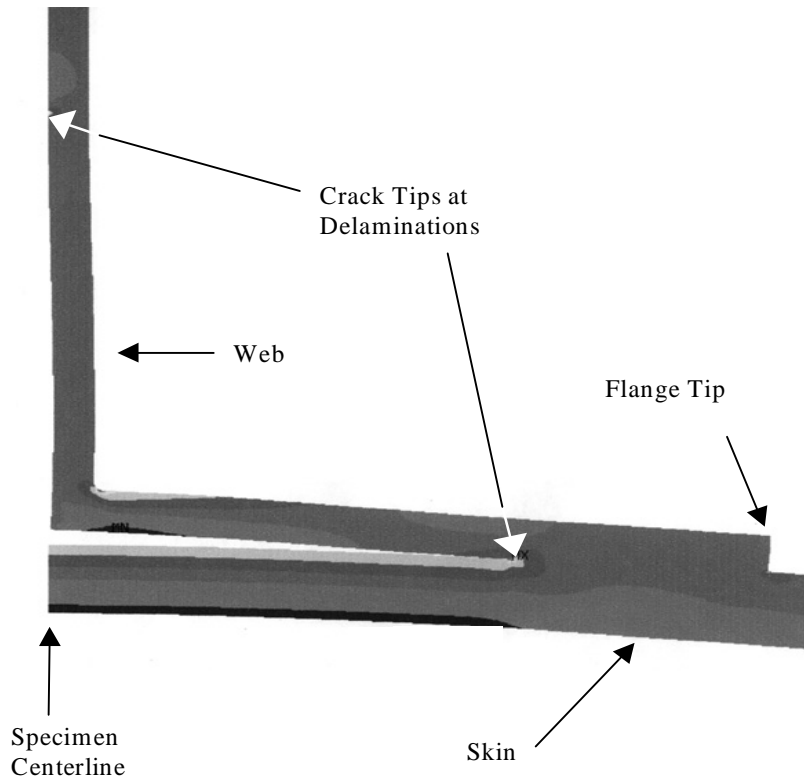
Figure 7. Plot of deformed skin/stiffener intersection region with delamination present (from ANSYS).
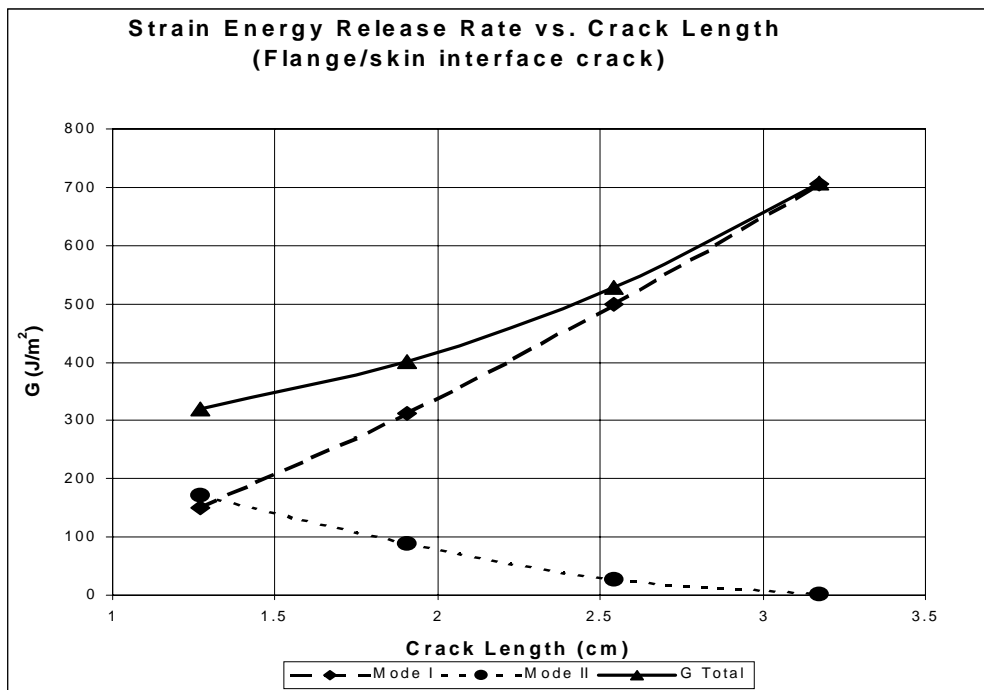

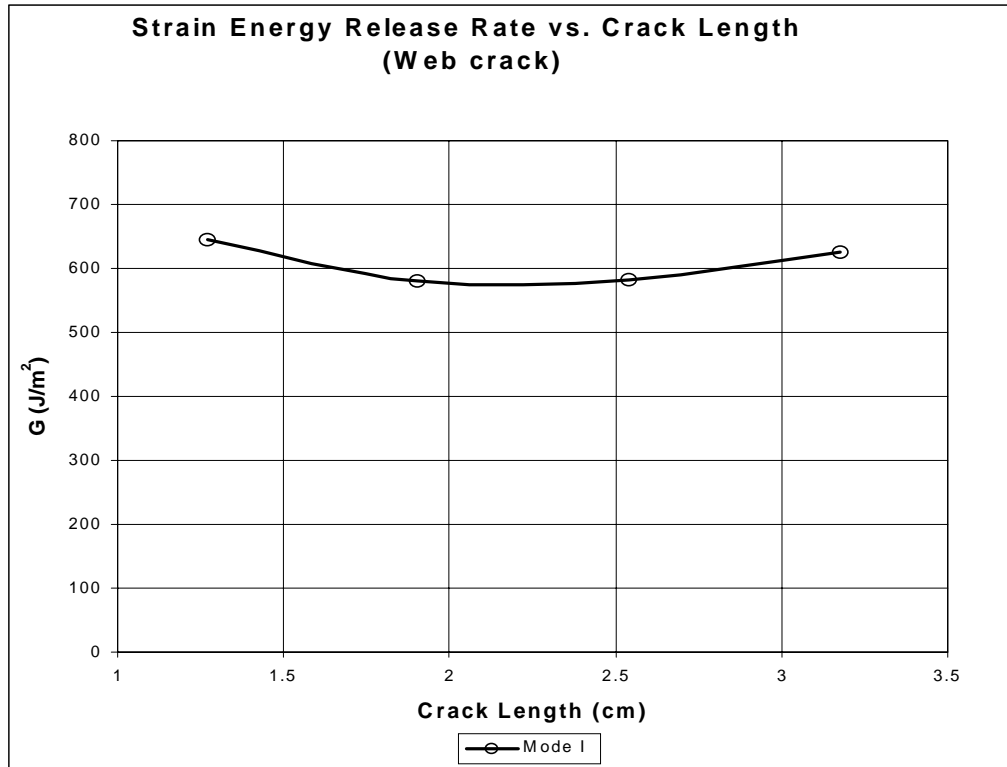Figure 8. SERR graph for flange/skin delamination (from ANSYS).

Figure 9. SERR graph for flange/skin delamination.